Detailed high-spin spectroscopy and the search for the wobbling mode in ^{171}Ta

D. J. Hartley, W. H. Mohr, and J. R. Vanhoy
Department of Physics, U.S. Naval Academy, Annapolis, Maryland 21402, USA

M. A. Riley, A. Aguilar, and C. Teal
Department of Physics, Florida State University, Tallahassee, Florida 32306, USA

R. V. F. Janssens, M. P. Carpenter, A. A. Hecht,* T. Lauritsen, E. F. Moore, and S. Zhu
Physics Division, Argonne National Laboratory, Argonne, Illinois 60439, USA

F. G. Kondev
Nuclear Engineering Division, Argonne National Laboratory, Argonne, Illinois 60439, USA

M. K. Djongolov, M. Danchev, and L. L. Riedinger
Department of Physics and Astronomy, University of Tennessee, Knoxville, Tennessee 37996, USA

G. B. Hagemann and G. Sletten
The Niels Bohr Institute, Blegdamsvej 17, DK-2100 Copenhagen, Denmark

P. Chowdhury and S. K. Tandel
Department of Physics, University of Massachusetts, Lowell, Massachusetts 01854, USA

W. C. Ma
Department of Physics, Mississippi State University, Mississippi State, Mississippi 39762, USA

S. W. Ødegärd
Department of Physics, University of Oslo, PB 1048 Blindern, N-0316 Oslo, Norway
(Received 26 September 2005; published 29 December 2005)

High-spin states in ^{171}Ta were populated in the ^{124}Sn(^{51}V,4n) reaction at 228 MeV to search for evidence of stable triaxial deformation. Identification of a wobbling sequence based on the previously known $\pi i_{13/2}$ structure would provide a unique signature for this rarely observed shape. No such sequence was identified in these data, which suggests that the island of triaxial strongly deformed bands may be smaller than once thought. However, over 200 new transitions and two new bands were placed in the level scheme and the sequence based on the $\pi i_{13/2}$ orbital could be observed up to spin and parity $I^{\pi} = (101/2^{+})$. The relative excitations of all the sequences were determined and the ground state of ^{171}Ta was found to have $5/2^{+}$ quantum numbers, contrary to previous reports. All of the previously known structures were extended to much higher spin and their high-frequency band crossings are interpreted within the framework of the cranked shell model.

DOI: 10.1103/PhysRevC.72.064325 PACS number(s): 21.10.Re, 23.20.Lv, 25.70.Gh, 27.70.+q

I. INTRODUCTION

The $i_{13/2}$ orbital has garnered considerable interest in high-spin studies as its intruder nature often causes a significant gain in deformation. Recently, the $\pi i_{13/2}$ sequences in light Lu nuclei have drawn attention because of the proposed wobbling structures based on this orbital [1–6]. Wobbling is a phenomenon unique to the rotation of a triaxially deformed nucleus and is perhaps the strongest evidence for a nucleus having a stable asymmetric shape [7]. As discussed by Hagemann and Hamamoto [8], the spinning of a triaxial nucleus allows for the collective rotation vector **R** to deviate from the axis of the largest moment of inertia, and this produces the wobbling motion. The amount **R** can deviate is quantized and is represented by a wobbling phonon quantum number ($n_w = 0, 1, 2, \ldots$). Therefore, a family of wobbling bands may exist based on the $n_w = 0$ sequence that, in the case of Lu, is the $\pi i_{13/2}$ structure. Because these sequences also have relatively large deformation, they are often referred to as triaxial strongly deformed (TSD) bands.

Ultimate cranker (UC) calculations reported in Schnack-Peterson *et al.* [9] suggested that a single-particle gap at $N = 94$ forms at large deformation ($\epsilon_2 \approx 0.39$) with a sizable degree of triaxiality ($\gamma \approx 20^{\circ}$). Thus, it was assumed that TSD bands would be observed in nuclei near $Z = 72$ and $N = 94$. Several strongly deformed (SD) structures were recently found in $N \approx 102$ Hf nuclei, and UC calculations indicate such bands likely exist in TSD minima. Eight SD sequences were observed

*Also at Department of Chemistry, University of Maryland, College Park, MD 20742.

in ^{174}Hf [10,11] and three in ^{172}Hf [12], which can be grouped into possible families based on similarities of their dynamic moments of inertia, but no conclusive evidence for wobbling could be extracted. In particular, the interband transitions that provide a clear signature for wobbling in the Lu isotopes are absent. It is therefore not clear whether the influence of triaxiality extends into the $N \approx 100$ region. It was this fact that provided the motivation for the present experiment on ^{171}Ta. The hafnium SD bands are likely based on more complex configurations [11,13] than a single $i_{13/2}$ proton as seen in the Lu isotopes; therefore, direct comparisons between the Hf and Lu bands may not be meaningful. The odd-A Ta nuclei provide a laboratory more similar to Lu in which one can determine whether a TSD shell gap occurs near $N = 100$. Because ^{171}Ta was the only tantalum isotope with a known $i_{13/2}$ sequence [14,15], it was chosen as the candidate to search for the wobbling mode.

As discussed below, there is no evidence for a wobbling sequence in ^{171}Ta. The implications of these results on the interpretation of the Hf bands and on the description of the "island" of TSD shapes are addressed. In addition, a significant extension of the ^{171}Ta level scheme is reported, where over 200 new transitions were added and two new bands were identified. New linking transitions between the sequences allowed for the excitation energies of all the structures to be determined for the first time. The ground state of ^{171}Ta can now be confirmed as a $5/2^+$ state. This is in contrast with two decay studies that suggested $7/2^+$ [16] and $5/2^-$ [17] ground-state assignments. High-frequency band crossings were also observed in each band and these have been interpreted with the cranked shell model.

II. EXPERIMENTAL DETAILS

High-spin states were populated in ^{171}Ta with the ^{124}Sn (^{51}V,4n) reaction at a beam energy of 228 MeV. The ^{51}V beam was provided by the ATLAS facility at Argonne National Laboratory. A beam intensity of $\sim$3 pnA was sustained throughout the experiment. The target consisted of two stacked ^{124}Sn self-supporting foils, each of $\sim$500 μg/cm^2 thickness. The Gammasphere array [18], which contained 100 Compton-suppressed Ge detectors at the time, detected the emitted γ radiation. A total of 2×10^9 events were collected when at least four γ rays were detected within prompt coincidence (defined by a software gate of $\sim$80 ns). These data were sorted into a Blue database [19] to facilitate quick creation of various coincidence histograms and spectra. In particular, Radware [20] cubes and hypercubes were created to inspect the γ-ray coincidence relationships.

The Blue database was also utilized to perform an angular correlation analysis to determine the spins of the states. Double gates on two known $E2$ transitions were placed and the resulting coincident γ rays were sorted into 16 different spectra corresponding to the different rings at which they were detected by Gammasphere. Background subtraction was performed utilizing the method of K. Starosta *et al.* [21]. An angular correlation ratio for the coincident γ rays was then calculated using $R_{\rm ang} = W(\theta_f, \phi)/W(\theta_{90^\circ}, \phi)$, where $W(\theta_f, \phi)$ is the intensity observed in the forward detectors ($\theta = 122^\circ$, 130°, 143°, 148°, and 163°) and $W(\theta_{90^\circ}, \phi)$ is the intensity observed in the Gammasphere rings near 90° ($\theta = 79^\circ$, 81°, 90°, 99°, and 101°). Both sets of rings are composed of an equal number of detectors. Normalized ratios of approximately 0.6 and 1.0 were observed for known stretched $E1$ and $E2$ transitions, respectively. When $R_{\rm ang}$ could not be measured, because of lack of statistics, spins were assigned assuming that the rotational behavior persists throughout the band, and the spins are shown in parentheses in the level scheme of Fig. 1. Table I lists the energy of the levels and γ rays, as well as the transition intensities and angular correlation ratios.

III. LEVEL SCHEME

Electron capture/beta (EC/β^+) decay studies of ^{171}W by Meissner *et al.* [17] suggested that the ground state of ^{171}Ta should be associated with the $5/2^-$ level of the $h_{9/2}$[541]1/2 band. In addition, the band-head states of the $g_{7/2}$[404]7/2, $h_{11/2}$[514]9/2, and $h_{11/2}$[523]7/2 sequences were determined to be located at 52.1, 236.3, and 530.8 keV, respectively. High-spin states of ^{171}Ta were evaluated by Bacelar *et al.* [15] using the same reaction as reported in this publication, but only six Ge detectors were utilized in the TESSA 2 array. Five rotational sequences were identified and configurations were assigned based on the characteristics of the bands. However, the only linking transitions observed were between the [514]9/2 and [404]7/2 bands, as well as between the $i_{13/2}$[660]1/2 and $d_{5/2}$[402]5/2 bands. Therefore, the relative excitation energies of the different proton orbitals remained unknown. In addition, the band head of the [514]9/2 sequence has been determined to be an isomer with a 46(3) ns lifetime [15], and its intrinsic quadrupole moment was measured to be 5.61 b by Dogra *et al.* [22]. The level scheme for ^{171}Ta deduced from the present data is displayed in Fig. 1. Tentative transitions and levels are shown as dashed lines in Fig. 1. Parities for the bands have never been directly measured; therefore, parity assignments are based on the configuration assignments discussed in Sec. IV.

A. Positive-parity structures

Band 1 was determined to be the ground-state sequence for ^{171}Ta through the various linking transitions displayed in Fig. 1. A partial level scheme is provided in Fig. 2 such that the low-spin portion is easier to read. This structure was observed previously and was associated with the [402]5/2 configuration [15]; thus, positive-parity and a band-head state of $I^\pi = 5/2^+$ were assigned. We are in agreement with this configuration assignment (see Sec. IV A1), and therefore the ground state of ^{171}Ta can be identified as $5/2^+$. This is in contrast with Meissner *et al.* [17], where a $5/2^-$ (from the [541]1/2 structure) ground state was suggested because of the observed allowed EC/β^+ decay from a $5/2^-$ state in ^{171}W with log ft $\geqslant 5.2$ to the supposed ground state in ^{171}Ta. A $5/2^+$ ground state for ^{171}Ta requires a first-forbidden decay from the $5/2^-$ ground state in ^{171}W; therefore, it is likely that the EC/β^+ decay observed by Meissner *et al.* strongly feeds the $5/2^-$ state of the [541]1/2 band located at 31.2 keV (see below) followed by an undetected 31-keV γ ray. The

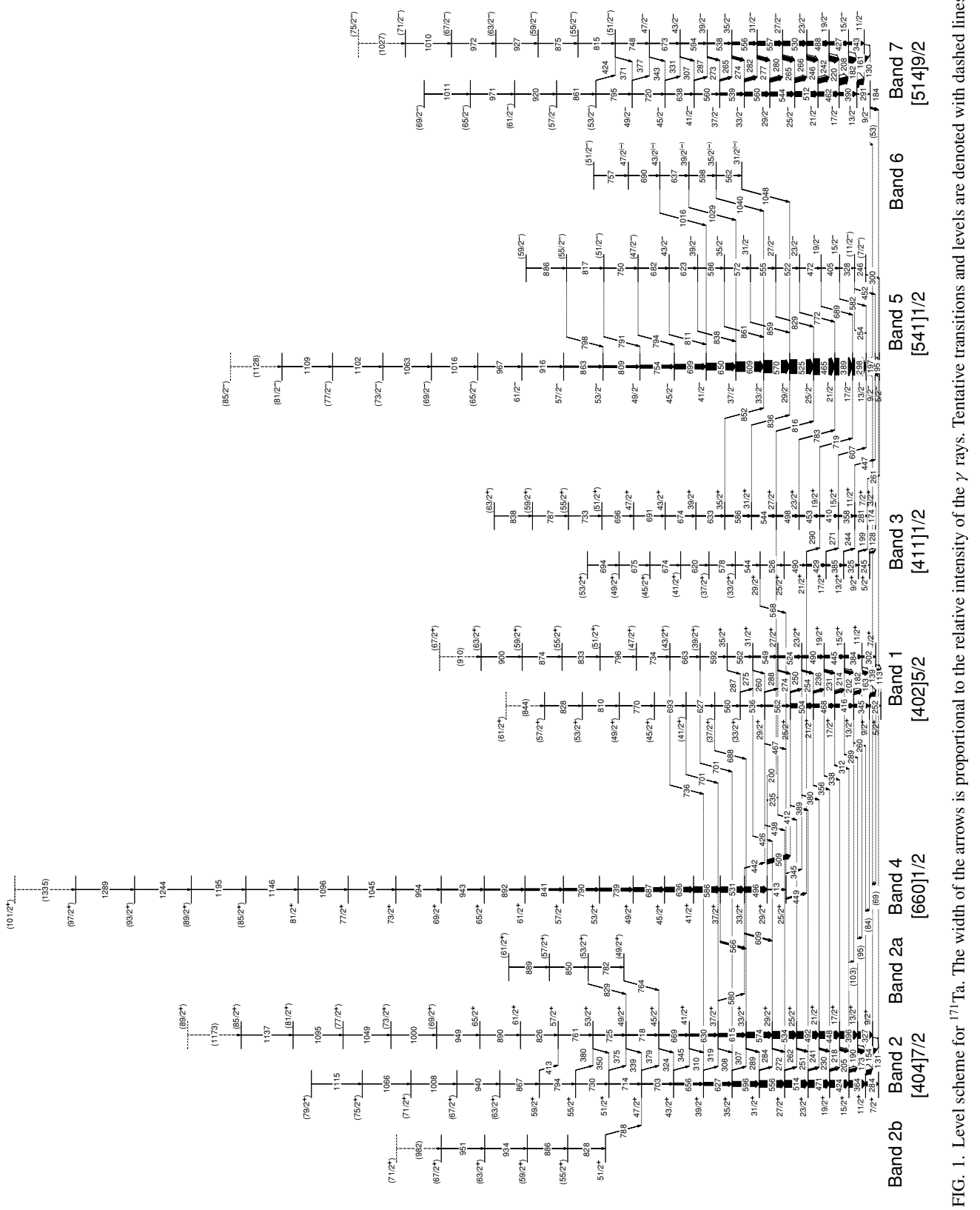

FIG. 1. Level scheme for ^{171}Ta. The width of the arrows is proportional to the relative intensity of the γ rays. Tentative transitions and levels are denoted with dashed lines.

TABLE I. γ-ray energies and intensities in ^{171}Ta.

I^{π}[a]	E_{level} (keV)	E_γ (keV)[b]	I_γ[c]	Ang. Corr. Ratio
		Band 1: [402]5/2 $\alpha = +1/2$		
$\frac{5}{2}^+$	0.0			
$\frac{9}{2}^+$	251.6	251.6	13.8(8)[d]	
		138.9	31(1)[d]	0.65(4)
$\frac{13}{2}^+$	596.5	344.9	18.3(8)	0.74(4)
		182.1	19.7(8)	0.63(4)
		260.4	2.5(2)	
$\frac{17}{2}^+$	1012.3	415.8	20(1)	0.89(5)
		213.8	14.6(7)	0.65(4)
		312.4	4.4(3)	0.36(5)
$\frac{21}{2}^+$	1479.9	467.6	21(1)	0.85(5)
		236.4	10.7(6)	0.69(4)
		356.5	2.7(2)	0.62(9)
$\frac{25}{2}^+$	1983.6	503.7	26(1)	0.88(4)
		249.8	6.9(4)	0.60(5)
		389.2	2.1(2)	0.64(8)
$\frac{29}{2}^+$	2545.7	562.1	8.8(7)	1.12(8)
		288.3	3.6(2)	0.71(6)
		437.7	0.9(1)	
		466.6	1.9(2)	1.1(1)
$(\frac{33}{2}^+)$	3081.5	535.8	6.1(4)	
		275.0	2.1(2)	
$(\frac{37}{2}^+)$	3641.1	559.6	4.9(5)	
		688.3	0.8(1)	
$(\frac{41}{2}^+)$	4268.1	627.0	3.3(2)	
		700.6	0.8(1)	
$(\frac{45}{2}^+)$	4961.5	693.4	1.9(2)	
$(\frac{49}{2}^+)$	5731.6	770.1	1.2(1)	
$(\frac{53}{2}^+)$	6542.0	810.4	0.7(1)	
$(\frac{57}{2}^+)$	7370.0	828.0	<0.5	
$(\frac{61}{2}^+)$	(8214)	(844)	<0.5	
		Band 1: [402]5/2 $\alpha = -1/2$		
$\frac{7}{2}^+$	112.6	112.6	~23[e]	0.63(6)
$\frac{11}{2}^+$	414.2	301.6	9.9(7)	0.60(7)
		162.7	21(1)	0.63(4)
$\frac{15}{2}^+$	798.2	384.0	16.7(9)	0.71(5)
		201.6	17.0(9)	0.63(5)
		289.4	3.2(2)	0.58(9)
$\frac{19}{2}^+$	1243.4	445.2	17.2(9)	0.88(6)
		231.3	12.5(6)	0.65(5)
		338.2	2.3(2)	0.54(7)
$\frac{23}{2}^+$	1733.7	490.3	16.0(9)	1.06(7)
		253.7	6.6(5)	0.80(8)
		380.4	2.2(2)	0.54(5)
$\frac{27}{2}^+$	2257.3	523.6	13.1(8)	1.1(1)
		273.9	5.1(4)	0.62(7)
		411.7	1.4(1)	
$\frac{31}{2}^+$	2806.3	549.0	9.7(7)	1.13(8)
		260.4	1.4(1)	
		425.6	<0.5	
$\frac{35}{2}^+$	3368.5	562.2	5.1(4)	1.12(8)
		287.0	0.6(1)	
$(\frac{39}{2}^+)$	3960.5	592.0	3.9(3)	
		700.9	0.8(1)	
$(\frac{43}{2}^+)$	4623.3	662.8	2.1(2)	
		736.4	0.7(1)	
$(\frac{47}{2}^+)$	5357.8	734.5	1.4(1)	
$(\frac{51}{2}^+)$	6153.3	795.5	0.9(1)	
$(\frac{55}{2}^+)$	6986.1	832.8	0.6(1)	
$(\frac{59}{2}^+)$	7860.1	874.0	<0.5	
$(\frac{63}{2}^+)$	8760	900	<0.5	
$(\frac{67}{2}^+)$	(9670)	(910)	<0.5	
		Band 2: [404]7/2 $\alpha = +1/2$		
$\frac{9}{2}^+$	181.8	130.7	~37[e]	0.69(4)
$\frac{13}{2}^+$	508.8	327.0	40(2)	0.75(4)
		173.4	24(1)	0.79(4)
$\frac{17}{2}^+$	904.9	396.1	42(2)	0.88(5)
		205.4	13.9(6)	0.78(4)
$\frac{21}{2}^+$	1353.2	448.3	42(2)	0.95(4)
		229.7	7.7(5)	0.81(6)
$\frac{25}{2}^+$	1845.5	492.3	42(2)	0.96(4)
		251.1	6.1(4)	0.78(6)
$\frac{29}{2}^+$	2379.7	534.2	43(2)	1.02(4)
		271.7	4.0(3)	0.71(6)
$\frac{33}{2}^+$	2953.2	573.5	33(2)	1.00(4)
		289.1	3.5(2)	
$\frac{37}{2}^+$	3568.0	614.8	22(1)	1.09(6)
		308.2	1.1(1)	
		579.7	4.1(4)	0.8(1)
$\frac{41}{2}^+$	4197.6	629.6	14(1)	
		310.5	2.2(2)	
$\frac{45}{2}^+$	4866.9	669.3	10.0(7)	1.03(8)
		323.9	1.8(1)	
$\frac{49}{2}^+$	5585.0	718.1	6.4(5)	1.12(9)
		339.3	1.1(1)	
$\frac{53}{2}^+$	6310.3	725.3	5.1(4)	1.19(9)
		349.9	0.7(1)	
$\frac{57}{2}^+$	7071.6	761.3	3.4(2)	0.95(8)
$\frac{61}{2}^+$	7897.3	825.7	2.0(1)	1.0(1)
$\frac{65}{2}^+$	8787.8	890.5	1.3(1)	1.1(1)
$(\frac{69}{2}^+)$	9736.4	948.6	0.7(1)	
$(\frac{73}{2}^+)$	10736.7	1000.3	<0.5	
$(\frac{77}{2}^+)$	11786.1	1049.4	<0.5	
$(\frac{81}{2}^+)$	12881.3	1095.2	<0.5	
$(\frac{85}{2}^+)$	14018	1137	<0.5	
$(\frac{89}{2}^+)$	(15191)	(1173)	<0.5	
		Band 2: [404]7/2 $\alpha = -1/2$		
$\frac{7}{2}^+$	51.4			
$\frac{11}{2}^+$	335.4	284.0	23.9(9)[d]	0.86(4)
		153.5	29(1)[d]	0.73(4)

TABLE I. *(Continued.)*

I^{π}[a]	E_{level} (keV)	E_{γ} (keV)[b]	I_{γ}^{c}	Ang. Corr. Ratio
$\frac{15}{2}^{+}$	699.5	364.1	41(2)	0.84(4)
		190.5	17.6(9)	0.83(5)
$\frac{19}{2}^{+}$	1123.4	423.9	43(2)	0.90(4)
		218.4	10.5(7)	0.77(6)
$\frac{23}{2}^{+}$	1594.2	470.8	44(2)	0.97(4)
		240.9	7.1(7)	0.77(5)
$\frac{27}{2}^{+}$	2107.9	513.7	43(2)	0.91(4)
		262.3	4.1(4)	0.88(7)
$\frac{31}{2}^{+}$	2663.9	556.0	41(2)	1.03(4)
		284.3	3.7(4)	
$\frac{35}{2}^{+}$	3259.7	595.8	31(2)	0.92(4)
		306.6	2.4(2)	
$\frac{39}{2}^{+}$	3887.1	627.4	20(1)	
		319.2	1.1(1)	
$\frac{43}{2}^{+}$	4542.8	655.7	12(1)	1.01(7)
		345.0	1.5(1)	
$\frac{47}{2}^{+}$	5245.4	702.6	6.2(5)	1.05(9)
		378.6	1.4(1)	
$\frac{51}{2}^{+}$	5959.8	714.4	4.1(3)	1.05(8)
		374.8	1.0(1)	
$\frac{55}{2}^{+}$	6689.8	730.0	2.5(2)	1.3(1)
		379.8	<0.5	
$\frac{59}{2}^{+}$	7483.7	793.9	2.4(2)	1.1(1)
		413	<0.5	
$(\frac{63}{2}^{+})$	8350.8	867.1	1.6(1)	
$(\frac{67}{2}^{+})$	9290.5	939.7	0.9(1)	
$(\frac{71}{2}^{+})$	10298.0	1007.5	0.5(1)	
$(\frac{75}{2}^{+})$	11364.5	1066.5	<0.5	
$(\frac{79}{2}^{+})$	12479.7	1115.2	<0.5	
		Band 2a		
$(\frac{49}{2}^{+})$	5631.1	764.2	0.6(1)	
$(\frac{53}{2}^{+})$	6413.6	782.5	<0.5	
		828.6	1.3(1)	
$(\frac{57}{2}^{+})$	7264.0	850.4	0.8(1)	
$(\frac{61}{2}^{+})$	8153	889	<0.5	
		Band 2b		
$\frac{51}{2}^{+}$	6033.9	788.5	1.2(1)	1.2(1)
$(\frac{55}{2}^{+})$	6861.8	827.9	1.0(1)	
$(\frac{59}{2}^{+})$	7747.4	885.6	0.8(1)	
$(\frac{63}{2}^{+})$	8681.9	934.5	0.6(1)	
$(\frac{67}{2}^{+})$	9633.0	951.1	<0.5	
$(\frac{71}{2}^{+})$	(10615)	(982)	<0.5	
		Band 3: [411]1/2 $\alpha = +1/2$		
$\frac{5}{2}^{+}$	246.6	128.3	∼1[e]	0.72(8)
$\frac{9}{2}^{+}$	491.7	245.1	3.4(3)	0.83(5)
		199.4	3.4(2)	0.58(4)
$\frac{13}{2}^{+}$	817.1	325.4	7.7(3)	0.77(4)
		243.5	2.6(3)	0.66(5)
$\frac{17}{2}^{+}$	1202.0	384.9	9.4(5)	0.79(5)
		270.9	2.0(1)	

TABLE I. *(Continued.)*

I^{π}[a]	E_{level} (keV)	E_{γ} (keV)[b]	I_{γ}^{c}	Ang. Corr. Ratio
$\frac{21}{2}^{+}$	1630.6	428.6	11.6(8)	1.06(5)
		289.7	1.8(1)	
$\frac{25}{2}^{+}$	2120.7	490.1	3.5(3)	0.77(6)
$\frac{29}{2}^{+}$	2647.0	526.3	3.0(2)	0.8(1)
		567.6	1.8(2)	
$(\frac{33}{2}^{+})$	3190.9	543.9	2.8(2)	
$(\frac{37}{2}^{+})$	3768.9	578.0	1.8(1)	
$(\frac{41}{2}^{+})$	4389.4	620.5	1.6(1)	
$(\frac{45}{2}^{+})$	5063.9	674.5	0.8(1)	
$(\frac{49}{2}^{+})$	5739.0	675.1	<0.5	
$(\frac{53}{2}^{+})$	6433	694	<0.5	
		Band 3: [411]1/2 $\alpha = -1/2$		
$\frac{3}{2}^{+}$	118.3			
$\frac{7}{2}^{+}$	292.2	173.9	13[d]	0.81(6)
		260.8	1.5[d]	
$\frac{11}{2}^{+}$	573.3	281.1	10.5(7)	0.81(4)
		447.1	1.5(1)	0.7(1)
$\frac{15}{2}^{+}$	930.9	357.6	9.4(5)	0.87(4)
		607.2	2.1(2)	0.72(5)
$\frac{19}{2}^{+}$	1340.8	409.9	9.4(5)	0.90(4)
		719.0	2.3(2)	0.64(5)
$\frac{23}{2}^{+}$	1793.7	452.9	9.2(5)	0.83(5)
		783.0	3.3(2)	0.59(6)
$\frac{27}{2}^{+}$	2291.8	498.1	9.7(6)	0.91(5)
		816.2	2.7(2)	0.66(8)
$\frac{31}{2}^{+}$	2836.0	544.2	9.2(6)	1.14(7)
		835.5	1.6(1)	
$\frac{35}{2}^{+}$	3422.0	586.0	7.9(5)	1.08(5)
		851.5	1.4(1)	
$\frac{39}{2}^{+}$	4054.7	632.7	5.5(4)	1.24(7)
$\frac{43}{2}^{+}$	4728.2	673.5	4.3(4)	1.01(7)
$\frac{47}{2}^{+}$	5418.9	690.7	2.6(2)	0.94(9)
$(\frac{51}{2}^{+})$	6114.7	695.8	1.8(2)	
$(\frac{55}{2}^{+})$	6847.9	733.2	1.2(1)	
$(\frac{59}{2}^{+})$	7635.2	787.3	0.8(1)	
$(\frac{63}{2}^{+})$	8473	838	<0.5	
		Band 4: [660]1/2		
$\frac{25}{2}^{+}$	2079.4	448.8	8.4(5)	0.95(4)
		345.5	<0.5	
$\frac{29}{2}^{+}$	2492.5	413.1	4.1(2)	0.94(5)
		508.9	25(1)	0.88(3)
		235.0	2.8(2)	0.76(9)
		200.5	0.8(1)	
$\frac{33}{2}^{+}$	2988.5	496.0	34(5)	0.88(4)
		608.8	6.9(5)	1.07(8)
		442.4	3.3(2)	
$\frac{37}{2}^{+}$	3519.0	530.5	34(1)	0.97(3)
		565.8	10.5(7)	0.94(6)
$\frac{41}{2}^{+}$	4105.3	586.3	35(1)	1.02(3)

TABLE I. *(Continued.)*

I^{π}[a]	E_{level} (keV)	E_γ (keV)[b]	I_γ^c	Ang. Corr. Ratio
$\frac{45}{2}^+$	4741.4	636.1	29(1)	1.02(3)
$\frac{49}{2}^+$	5428.6	687.2	25(1)	1.07(4)
$\frac{53}{2}^+$	6167.1	738.5	19(1)	1.08(4)
$\frac{57}{2}^+$	6957.2	790.1	14.4(7)	1.18(4)
$\frac{61}{2}^+$	7798.6	841.4	11.8(6)	0.95(4)
$\frac{65}{2}^+$	8691.0	892.4	8.0(5)	1.08(4)
$\frac{69}{2}^+$	9634.4	943.4	6.1(4)	1.08(5)
$\frac{73}{2}^+$	10628.7	994.3	3.4(3)	1.04(7)
$\frac{77}{2}^+$	11674.0	1045.3	2.2(2)	1.2(1)
$\frac{81}{2}^+$	12770.2	1096.2	1.2(1)	0.9(1)
$(\frac{85}{2}^+)$	13916.1	1145.9	0.7(1)	
$(\frac{89}{2}^+)$	15110.7	1194.6	<0.5	
$(\frac{93}{2}^+)$	16354.6	1243.9	<0.5	
$(\frac{97}{2}^+)$	17644	1289	<0.5	
$(\frac{101}{2}^+)$	18979	1335	<0.5	
Band 5: [541]1/2 $\alpha = +1/2$				
$\frac{5}{2}^-$	31.2			
$\frac{9}{2}^-$	126.3	95.1	∼22[e]	0.62(5)
$\frac{13}{2}^-$	323.6	197.3	83(4)	0.76(3)
$\frac{17}{2}^-$	621.8	298.2	97(4)	0.86(3)
$\frac{21}{2}^-$	1010.7	388.9	100(4)	0.92(2)
$\frac{25}{2}^-$	1475.6	464.9	97(4)	0.99(2)
$\frac{29}{2}^-$	2000.3	524.7	85(4)	1.03(2)
$\frac{33}{2}^-$	2570.4	570.1	75(3)	1.01(2)
$\frac{37}{2}^-$	3178.9	608.5	59(3)	1.01(2)
$\frac{41}{2}^-$	3829.0	650.1	43(2)	1.05(3)
$\frac{45}{2}^-$	4528.2	699.2	29(1)	1.04(3)
$\frac{49}{2}^-$	5281.7	753.5	19.2(8)	1.08(4)
$\frac{53}{2}^-$	6090.5	808.8	12.2(5)	1.11(5)
$\frac{57}{2}^-$	6953.3	862.8	9.0(4)	1.18(7)
$\frac{61}{2}^-$	7868.8	915.5	5.4(3)	1.00(9)
$(\frac{65}{2}^-)$	8835.7	966.9	3.4(2)	0.9(1)
$(\frac{69}{2}^-)$	9851.7	1016.0	2.1(1)	
$(\frac{73}{2}^-)$	10914.4	1062.7	1.4(1)	
$(\frac{77}{2}^-)$	12016.3	1101.9	0.6(1)	
$(\frac{81}{2}^-)$	13125.2	1108.9	<0.5	
$(\frac{85}{2}^-)$	(14253)	(1128)	<0.5	
$(\frac{7}{2}^-)$	331.3	300.1	<0.5[e]	
$(\frac{11}{2}^-)$	577.7	246.4	<0.5	
		451.7	0.8(1)	
		254.2	<0.5	

TABLE I. *(Continued.)*

I^{π}[a]	E_{level} (keV)	E_γ (keV)[b]	I_γ^c	Ang. Corr. Ratio
Band 5: [541]1/2 $\alpha = -1/2$				
$\frac{15}{2}^-$	905.5	327.8	1.1(1)	
		581.9	0.8(1)	0.48(7)
$\frac{19}{2}^-$	1310.9	405.4	1.7(2)	
		689.4	1.1(1)	0.41(6)
$\frac{23}{2}^-$	1782.7	471.8	2.5(3)	1.0(1)
		771.8	2.3(3)	
$\frac{27}{2}^-$	2304.8	522.1	3.4(4)	1.5(2)
		829.3	2.3(3)	0.27(6)
$\frac{31}{2}^-$	2859.4	554.6	4.7(4)	
		858.8	2.2(3)	0.39(7)[f]
$\frac{35}{2}^-$	3431.4	572.0	4.1(4)	
		860.9	2.4(3)	0.39(7)[f]
$\frac{39}{2}^-$	4017.1	585.7	3.1(3)	1.2(1)
		837.8	2.9(3)	0.68(8)
$\frac{43}{2}^-$	4640.5	623.4	2.9(3)	1.3(1)
		811.2	1.7(2)	
$(\frac{47}{2}^-)$	5322.6	682.1	4.3(5)	
		794.1	1.6(2)	
$(\frac{51}{2}^-)$	6072.2	749.6	3.8(4)	
		790.7	1.3(2)	
$(\frac{55}{2}^-)$	6888.8	816.6	1.7(2)	
		798.2	0.6(1)	
$\frac{59}{2}^-$	7775	886	<0.5	
Band 6				
$\frac{31}{2}^{(-)}$	3048.3	1048.0	2.5(2)	0.37(4)
$\frac{35}{2}^{(-)}$	3610.3	562.0	1.4(1)	0.86(7)
		1039.9	2.4(2)	
$\frac{39}{2}^{(-)}$	4208.0	597.7	2.8(3)	1.1(1)
		1029.0	1.9(2)	
$\frac{43}{2}^{(-)}$	4845.1	637.1	3.0(3)	0.78(8)
		1016.1	1.5(2)	
$\frac{47}{2}^{(-)}$	5535.6	690.5	2.4(3)	1.2(1)
$(\frac{51}{2}^-)$	6292.7	757.1	1.2(1)	
Band 7: [514]9/2 $\alpha = +1/2$				
$\frac{9}{2}^-$	235.0	183.6	N/D	0.67(5)
$\frac{13}{2}^-$	526.3	291.3	3.7(4)	0.75(6)
		160.7	45(2)	0.71(3)
$\frac{17}{2}^-$	916.0	389.7	21(1)	0.87(3)
		207.7	41(2)	0.73(3)
$\frac{21}{2}^-$	1378.0	462.0	26(1)	0.91(4)
		242.3	29(1)	0.75(3)
$\frac{25}{2}^-$	1889.5	511.5	31(1)	0.86(6)
		265.5	24(1)	0.69(3)[f]
$\frac{29}{2}^-$	2434.0	544.5	26(1)	1.11(7)
		279.6	21(1)	0.72(7)
$\frac{33}{2}^-$	2993.5	559.5	25(1)	1.04(5)[f]
		282.2	16.2(8)	0.76(5)
$\frac{37}{2}^-$	3532.4	538.9	15(1)	1.05(4)[f]
		265.4	8.1(6)	0.69(3)[f]

TABLE I. *(Continued.)*

I^{π}[a]	E_{level} (keV)	E_{γ} (keV)[b]	I_{γ}^{c}	Ang. Corr. Ratio
$\frac{41}{2}^-$	4092.9	560.5	6.1(6)	1.04(5)[f]
		287.3	3.4(3)	0.67(4)
$\frac{45}{2}^-$	4730.7	637.8	5.6(4)	1.12(7)
		330.9	2.8(2)	0.67(5)
$\frac{49}{2}^-$	5450.5	719.8	3.6(2)	1.1(1)
		377.3	0.9(1)	
$(\frac{53}{2}^-)$	6245.5	795.0	2.7(2)	
		424	<0.5	
$(\frac{57}{2}^-)$	7106.8	861.3	1.5(1)	
$(\frac{61}{2}^-)$	8026.3	919.5	0.9(1)	
$(\frac{65}{2}^-)$	8997.0	970.7	0.6(1)	
$(\frac{69}{2}^-)$	10008	1011	<0.5	
	Band 7: [514]9/2 $\alpha = -1/2$			
$\frac{11}{2}^-$	365.5	130.5	∼38[d]	0.71(3)
$\frac{15}{2}^-$	708.1	342.6	18(1)	0.88(4)
		181.9	39(2)	0.77(2)[f]
$\frac{19}{2}^-$	1135.4	427.3	21(1)	0.95(3)
		219.5	32(1)	0.74(3)
$\frac{23}{2}^-$	1623.8	488.4	27(1)	0.91(4)
		245.8	25(1)	0.74(4)
$\frac{27}{2}^-$	2154.3	530.5	28(1)	0.89(6)
		264.8	23(1)	0.69(3)[f]
$\frac{31}{2}^-$	2711.4	557.1	26(1)	0.86(4)[f]
		277.2	17.5(9)	0.72(7)
$\frac{35}{2}^-$	3267.1	555.7	16(1)	0.86(4)[f]
		273.6	12.7(6)	0.64(3)[f]
$\frac{39}{2}^-$	3805.6	538.5	6.5(4)	1.05(4)[f]
		273.1	5.4(3)	0.64(3)[f]
$\frac{43}{2}^-$	4399.9	594.3	6.1(4)	0.87(4)
		306.6	2.6(2)	0.59(3)
$\frac{47}{2}^-$	5073.3	673.4	4.1(3)	0.91(5)
		342.6	1.3(1)	
$(\frac{51}{2}^-)$	5821.8	748.5	2.9(4)	
		371.1	0.8(1)	
$(\frac{55}{2}^-)$	6637.1	815.3	1.9(2)	
$(\frac{59}{2}^-)$	7511.9	874.8	1.5(1)	
$(\frac{63}{2}^-)$	8438.8	926.9	1.2(1)	
$(\frac{67}{2}^-)$	9411.0	972.2	0.7(1)	
$(\frac{71}{2}^-)$	10420.9	1009.9	<0.5	
$(\frac{75}{2}^-)$	(11448)	(1027)	<0.5	

[a]Spin and parity of the depopulated state.
[b]Uncertainties in γ-ray energy are 0.2 keV for most transitions, except for relatively weak transitions (<1) where 0.5 keV uncertainties are appropriate.
[c]Relative intensity of the transition with respect to the intensity of the 388.9-keV transition.
[d]Estimated based on intensity balance and branching ratio.
[e]Estimated based on intensity balance.
[f]Unresolved doublet.

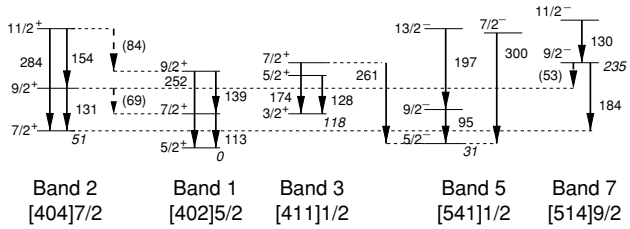

FIG. 2. Partial level scheme for ^{171}Ta highlighting the low-spin states. Note that the band-head energies are indicated in italics.

new assignment also disagrees with the assumption of a $7/2^+$ ground state by Ladenbauer-Bellis and Rezanka [16] to explain the EC/β^+-decay feeding of ^{171}Hf from ^{171}Ta. Baglin [23] recently noted that the strongest branches to ^{171}Hf were the

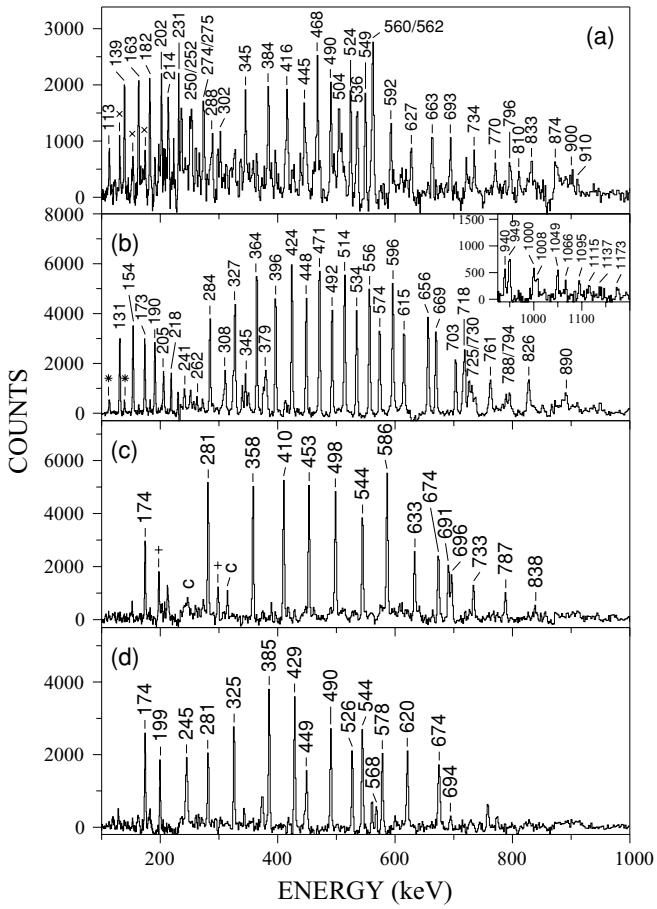

FIG. 3. Unless otherwise indicated, the spectra shown are the result of a sum of all triple coincidence gates using $E2$ transitions. (a) Spectrum of Band 1 ([402]5/2), where the crosses indicate transitions from Band 2. (b) Spectrum of Band 2 ([404]7/2), where the asterisks denote transitions from Band 1. All triple combinations with the 627- and 630-keV transitions were summed to produce this spectrum. The inset displays the high-energy transitions and was produced by triple gates on the highest energies within the band. (c) Spectrum of the $\alpha = -1/2$ signature of Band 3 ([411]1/2), where the pluses indicate transitions from Band 5 and the transitions marked with C are known contaminants. (d) Spectrum of the $\alpha = +1/2$ signature of Band 3.

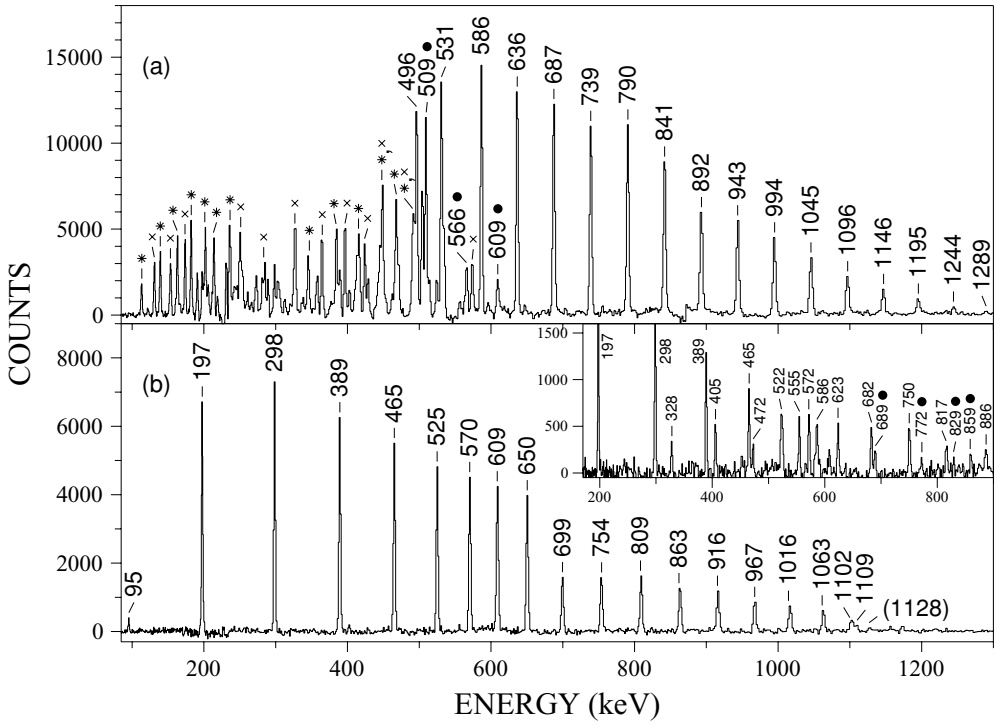

FIG. 4. (a) Spectrum of Band 4 ([660]1/2), which results from summing all triple coincidence gates on in-band transitions. Peaks marked with an asterisk or a cross indicate the transition is from Band 1 or 2, respectively. Transitions denoted with a filled circle are linking transitions. (b) Spectrum of the $\alpha = +1/2$ signature of Band 5 ([541]1/2) produced in a similar manner as panel (a). The inset displays the $\alpha = -1/2$ signature of Band 5, where linking transitions are denoted with filled circles.

$(3/2^-)$, $(5/2^-)$, and $(7/2^-)$ states, which is consistent with a $5/2^-$ ground state. However, it is unlikely that the $5/2^-$ state at 31.2 keV would EC/β^+ decay because it is allowed to γ decay to the ground state. With this new assignment, perhaps the EC/β^+ decay spectrum of ^{171}Ta needs to be reconsidered. Band 1 was extended from $35/2^+$ to a tentative spin of $(67/2^+)$, as seen in Fig. 1, and a sample spectrum is provided in Fig. 3(a). Several linking transitions from Band 1 to Band 2 were observed, which is indicative that the two bands likely share the same parity and have overlapping wave functions.

The linking transitions from Band 1 to Band 2 fix the band-head level of the latter at 51.4 keV. Several of these linking transitions were measured to have angular correlation ratios consistent with dipole character (see Table I). A relative spin assignment can be made, which suggests that the band-head state for Band 2 is $I^\pi = 7/2^+$. This assignment is consistent with Band 2 having the [404]7/2 configuration as stated in Ref. [15] and the band-head level is roughly within agreement with the [404]7/2 state reported in Ref. [17] (52.1 keV). A sample spectrum shown in Fig. 3(b) displays how the band was extended to high spin (from $43/2^+$ to $89/2^+$). The spectrum additionally demonstrates the coincidence with the low-spin portion of Band 1. No linking transitions could be directly observed, but the likely low-energy, highly converted transitions are tentatively placed in Fig. 1 connecting Band 2 to Band 1. A 579.7-keV linking transition is also found decaying from the $37/2^+$ state to the $33/2^+$ level in Band 4. Two sequences, labeled Bands 2a and 2b in Fig. 1, were observed to feed into Band 2 at $45/2^+$ and $47/2^+$, respectively. An angular correlation ratio of 1.2(1) for the 788.5-keV linking transition confirms the spin assignment for Band 2b.

The sequence labeled Band 3 in Fig. 1 was newly identified in the present data. Unlike the first two structures, Band 3 does not exhibit a strongly coupled character and spectra for the $\alpha = -1/2$ and +1/2 signatures are given in Figs. 3(c) and (d), respectively. The 448.8-keV linking transition from the $25/2^+$ state in Band 4 (see below) was determined to have an $E2$ character, thus allowing the spin assignment shown in Fig. 1 and requiring that the band has positive parity. An energy of 118.3 keV was determined for the lowest state, which has $3/2^+$ quantum numbers. Band 3 is linked with Band 5 through a series of transitions that were determined to be nearly pure dipoles based on their angular correlation ratio (see Table I). These transitions are assumed to be $E1$ in nature as Band 5 has been assigned negative parity.

Band 4 was previously identified and linked to Band 1 through the 508.9-keV transition [15]. The decay out of the band was determined to be more complex as seven new linking transitions are observed which feed Bands 2 and 3 as well. The angular correlation analysis confirms $E2$ character for the 442.4-, 508.9-, 565.8-, and 608.8-keV linking transitions, thus, firmly establishing the spin assignment proposed in Fig. 1 and the positive parity. The fragmented decay is similar to the [660]1/2 bands in ^{165,167}Lu [4,5]. Indeed, Bacelar *et al.* [15] assigned this configuration to this sequence and observed it up to $I^\pi = 69/2^+$. The present data allowed for the extension of the band to $(101/2^+)$ and a spectrum is provided in Fig. 4(a).

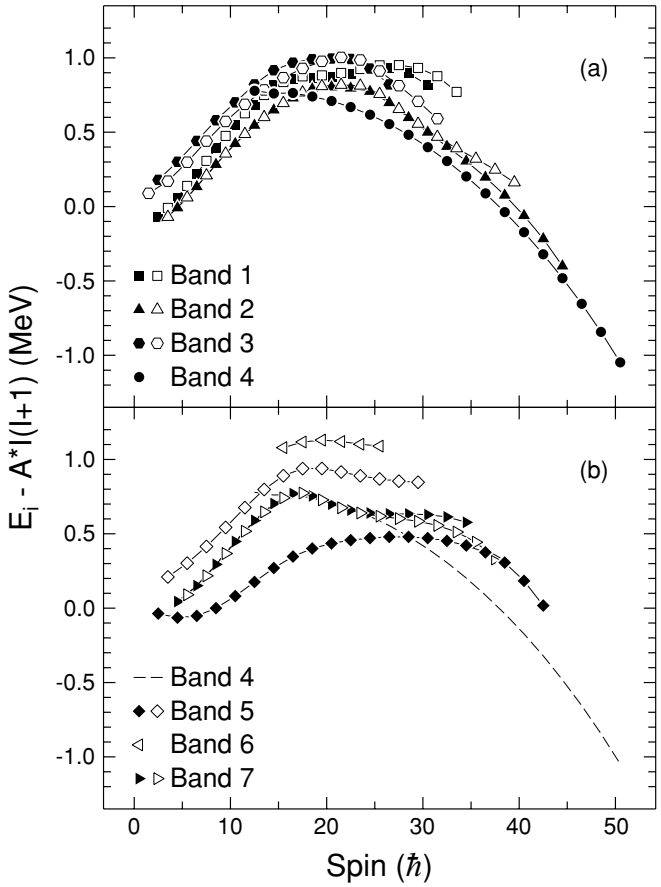

FIG. 5. Excitation energies of the observed levels minus a rigid-rotor reference where this reference was assumed to have a moment of inertia parameter $A = 0.0077$ MeV. The positive-parity sequences are displayed in (a), whereas the negative-parity structures are in (b). Band 4 is also displayed in (b) as a dashed line for reference. Positive (negative) signatures are represented with filled (open) symbols.

In this spectrum, one may also observe the various coincident transitions from Bands 1 and 2 because of the strong feeding of these structures. By inspection of Fig. 4(a), the remarkable regularity of the band may be noticed with it having nearly constant energy spacings of ∼51 keV from $37/2^+$ to $93/2^+$. As seen in Fig. 5, which plots the level energies minus a rigid reference, Band 4 becomes the yrast sequence at $I = 61/2$ and remains so up to its highest state.

B. Negative-parity bands

The favored signature of Band 5 makes up the yrast sequence for ^{171}Ta below 61/2 [see Fig. 5(b)] and has been associated with the [541]1/2 orbital [15], thus negative parity is implied for these states. The dipole transitions from Band 3 confirm the previously suggested spins that had been based on systematics of similar bands in heavier Ta nuclei. The band-head state was determined to be at 31.2 keV with a spin and parity of $5/2^-$. Figure 4(b) provides a spectrum of this sequence and illustrates how the band was extended from $69/2^-$ to $(85/2^-)$. In addition, the unfavored signature partner was identified and connected to the favored sequence through a series of dipole transitions. Large signature splitting is evident in Fig. 5(b) with an energy difference of approximately 500 keV, which is characteristic of the [541]1/2 orbital. This unfavored sequence could be observed up to a spin of $59/2^-$, and a spectrum of it is shown in the inset of Fig. 4(b).

Band 6 is also observed for the first time in this experiment, and it feeds Band 5 through a series of high-energy linking transitions. The 1048.0-keV line was measured to have an angular correlation ratio of 0.37(4), suggesting dipole character. Thus, the 3048.3-keV state of Band 6 has been assigned a spin of 31/2, but the assigned negative parity must be regarded as tentative as a configuration cannot be confidently assigned. A spectrum of this structure is presented in Fig. 6(a), with the linking transitions highlighted in its inset.

As stated above, the band-head level of Band 7 was found to be isomeric, with $T_{1/2} = 46(3)$ ns, and this sequence was associated with the [514]9/2 proton [15]. The 183.6-keV linking transition from the band-head state to the $7/2^+$ state in Band 2 (as seen in Figs. 1 and 2) fixes the excitation energy of this sequence to be 235.0 keV, which is in general agreement with Meissner *et al.* [17] who placed the [514]9/2 level at 236.3 keV. An angular correlation ratio of 0.67(5) was determined for this linking transition to the $7/2^+$ state in Band 2, and this observation indicates that a spin of 9/2 is appropriate for the band head. The negative parity is assumed based on the configuration assignment. Meissner *et al.* also observed a 53.4-keV γ ray from the $9/2^-$ state to the $7/2^+$ state in Band 2. Although this low-energy transition could not be directly confirmed, the 130.5-keV γ ray from Band 7 was found to be in coincidence with the 130.7-keV line in Band 2. This is consistent with the presence of a 53-keV transition between the bands such that this transition is also indicated in Figs. 1 and 2. Figure 6(b) displays a sample spectrum of Band 7 that confirms the extension of the structure from $39/2^-$ to $(75/2^-)$.

IV. DISCUSSION

Woods-Saxon calculations [24] indicate that the $d_{5/2}[402]5/2$, $g_{7/2}[404]7/2$, $d_{3/2}[411]1/2$, $h_{11/2}[514]9/2$, $h_{9/2}[541]1/2$, and $i_{13/2}[660]1/2$ orbitals are near the Fermi surface for ^{171}Ta with a deformation of $\beta_2 \approx 0.24$. Using this information along with alignment plots in Fig. 7, $B(M1)/B(E2)$ ratios in Fig. 8, and the assignments of Bacelar *et al.* [15], configurations for each of the bands in ^{171}Ta have been proposed. It should be noted that the Harris parameters $\mathcal{J}_0 = 29\,\hbar^2$/MeV and $\mathcal{J}_1 = 60\,\hbar^4$/MeV^3 used in Fig. 7 were selected to produce a nearly constant alignment in the [514]9/2 structure (Band 7) following the first crossing [see Fig. 7(d)]. This was done such that the higher-frequency crossings could be examined more accurately. Theoretical $B(M1)/B(E2)$ ratios shown in Fig. 8 were calculated using the geometric model of Dönau and Frauendorf [25]. The g_R value was taken to be Z/A and the g_Ω values were calculated using a Woods-Saxon potential and these values are summarized in Table II. A quadrupole moment of 6.0 b was also assumed for these calculations based on a $\beta_2 = 0.24$ deformation.

TABLE II. Parameters used in calculating theoretical $B(M1)/B(E2)$ values shown in Fig. 8.

Configuration	g_Ω	K	i_x
$\pi[402]5/2$	1.57	2.5	0.0
$\pi[404]7/2$	0.61	3.5	0.0
$\pi[514]9/2$	1.30	4.5	1.6
$\pi[411]1/2$	−1.23	0.5	0.0
νAB	−0.30	0.0	9.3
νA	−0.30	2.5	5.0
νE	−0.38	2.5	0.0
νBC	−0.30	0.0	3.4

A. Positive-parity bands

1. The band based on the [402]5/2 orbital

Bacelar *et al.* [15] assigned Band 1 as the [402]5/2 configuration. As seen in Fig. 8(a), the calculated $B(M1)/B(E2)$ values for this configuration (shown as a solid line) are consistent with the experimental values for Band 1. Therefore, we are in agreement with the previous assignment of Band 1. However, one may note that the experimental values are systematically less than the calculated ones. This is likely because of the mixing with Band 2, whose $B(M1)/B(E2)$ ratios are found to be much lower [see Fig. 8(a)]. Indeed, Band 2, which is assigned to the [404]7/2 configuration, is the pseudospin partner [26] of Band 1. The $B(M1)_{\text{inter}}/B(M1)_{\text{intra}}$ ratios were determined from the linking transitions between Band 1 and 2 and are given in Fig. 9. These ratios indicate that the mixing between the wave functions of the bands is nearly 10% over a large range of spins. Because the [404]7/2 sequence has much lower $B(M1)/B(E2)$ ratios, the mixing results in a lowering of the ratios for the [402]5/2 band, as observed in Fig. 8.

The alignment for Band 1 is displayed in Fig. 7(a), where two crossings can be clearly observed. The first occurs at a frequency of ∼0.27 MeV with an alignment gain of 9.3$\hbar$. This crossing is well documented throughout the rare-earth nuclei and is assigned to the alignment of the two lowest $i_{13/2}$ neutrons and is commonly referred to as the *AB* crossing [27]. These crossing frequency and alignment gain values are similar to those seen in the ground-state bands in the even-even neighbors ^{170}Hf [28] ($\hbar\omega_c \approx 0.26$ MeV, $\Delta i_x \approx 9.1\hbar$), which is shown in Fig. 7(d), and ^{172}W [29] ($\hbar\omega_c \approx 0.25$ MeV, $\Delta i_x \approx 8.8\hbar$). Cranked shell-model (CSM) calculations were performed, with deformation parameters of $\beta_2 = 0.24$, $\beta_4 = 0$, and $\gamma = 1^\circ$, and predict an *AB* crossing frequency of ∼0.21 MeV. Jensen *et al.* [30] performed a series of CSM calculations for the region near ^{171}Ta and found that the predicted values are systematically lower on average by 45 keV than experiment, which is consistent with the present results. As suggested by Jensen *et al.* [30], the discrepancy may result from improper pairing energies or perhaps higher-order terms (i.e., quadrupole-quadrupole pairing) are needed to accurately predict this crossing. In addition, a change in deformation following the alignment could also affect the crossing frequency, whereas the CSM assumes a constant deformation throughout the crossing region.

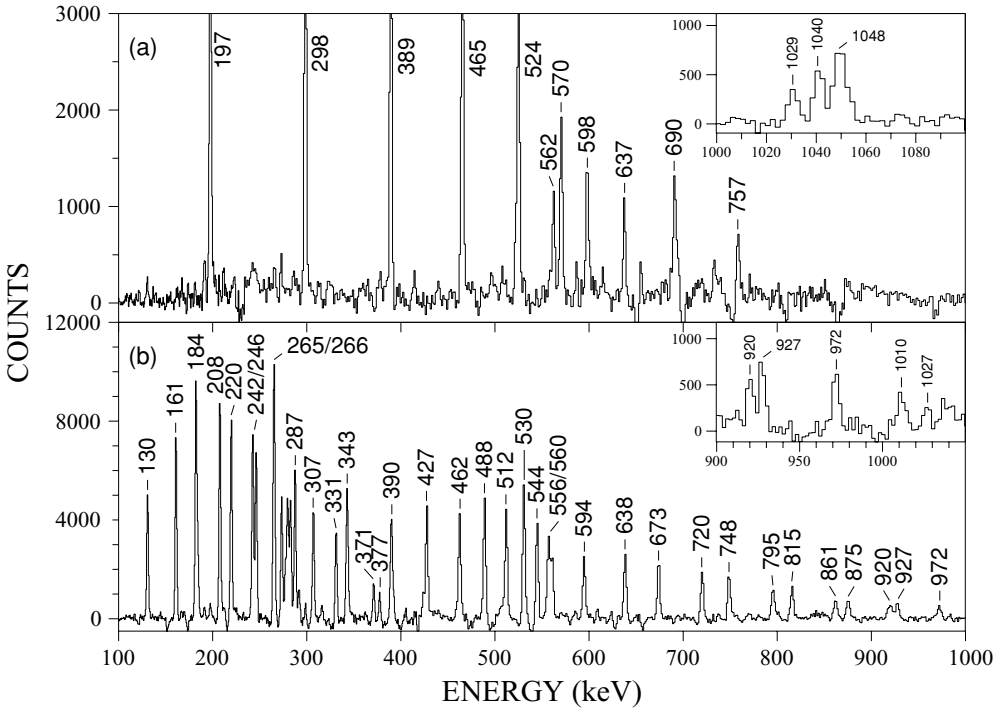

FIG. 6. (a) Spectrum of band 6 from summing triple gates using any two of the 197-, 298-, 389-, 465-, and 524-keV transitions with the 562-, 598-, and 637-keV transitions. The inset is from the same spectrum and displays the linking transitions. (b) Spectrum of Band 7 ([514]9/2) resulting from the sum of two double gates (538/556 + 539/560). The inset shows the extension of the band to its highest spins and results from the summing of many triple gates at the top of the band.

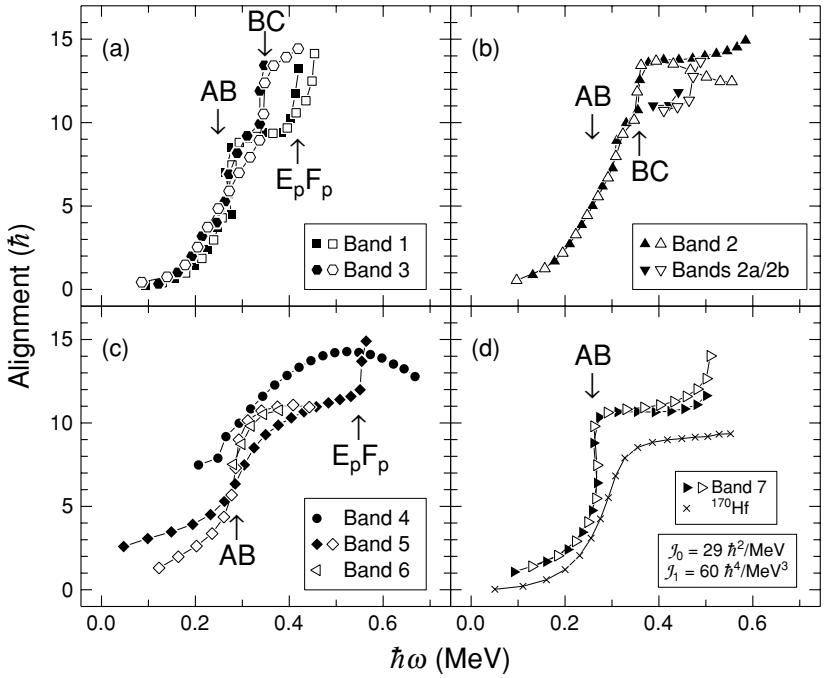

FIG. 7. Alignments for the bands in ^{171}Ta. Harris parameters of $\mathcal{J}_0 = 29\,\hbar^2$/MeV and $\mathcal{J}_1 = 60\,\hbar^4$/MeV^3 were used to subtract the angular momentum of the rotating core. Observed crossings are designated in the figure. Filled (empty) symbols denote a $\alpha = +1/2\ (-1/2)$ sequence.

A second crossing in Band 1 is observed near a frequency of 0.42 MeV with an alignment gain larger than $4.7\hbar$. The next available crossing predicted by the CSM is based on the alignment of the lowest two $h_{11/2}$ quasiprotons. Figure 10 displays the CSM calculation for quasiprotons where the E_pF_p crossing (associated with the $h_{11/2}$ protons) is found at ∼0.45 MeV, in good agreement with the data. One may note that the ground-state band in ^{170}Hf, shown in Fig. 7(d), does not observe this crossing even though this alignment is expected. The fact that Ta is an odd-Z nucleus means that the proton pairing energy will be slightly reduced, as compared with the even-even nucleus, resulting in a lower crossing frequency for the odd-Z case. However, it is not likely that this effect alone would account for the >100 keV difference in crossing frequency; therefore, the delay seen in the even-even nuclei is not well understood.

2. The band based on the [404]7/2 orbital

As previously mentioned, Band 2 was assigned the [404]7/2 configuration in Ref. [15]. Indeed, the $B(M1)/B(E2)$ ratios at low spin agree with theoretical predictions [see Fig. 8(a)], although the experimental values are slightly larger because of the mixing with the [402]5/2 band as described above. Band 2 has a different alignment pattern, shown in Fig. 7(b), as compared with the [402]5/2 sequence. The AB crossing is observed at a frequency near 0.26 MeV, but it is much more gradual than that seen in Band 1. This low-frequency gradual alignment has been observed in sequences throughout the region and has been explained as a consequence of a shape change caused by the crossing with a more-deformed band [31]. The more-deformed structure is the result of a pair of protons scattering into the deformation driving $h_{9/2}$ orbital. Note that this is not an alignment, but a promotion of a pair of protons into the $h_{9/2}$ orbital. This may cause the sequence to have an increased deformation relative to its initial value.

A second alignment is observed in Band 2 at ∼0.35 MeV, as seen in Fig. 7(b), but no other crossing is observed following this alignment. Similar behavior is found in the [404]7/2 bands in ^{163,165}Lu [2,32], where it has been suggested that the $g_{7/2}$ structures are crossed by a three-quasiparticle band having a configuration of an $h_{11/2}$ proton coupled with the $AE(F)$ neutrons (where E and F are likely from the [512]5/2 neutron orbital and exhibit little signature splitting [33,34]). This crossing is stated to occur during the AB alignment and, then, a crossing near 0.32 MeV in these Lu nuclei is because of the BC alignment [2,32]. It appears that the same scenario occurs in ^{171}Ta, where the [404]7/2 sequence is crossed by the $\pi h_{11/2}\nu AE(F)$ structure before the AB alignment is completed and the crossing observed at 0.35 MeV is because of the aligning BC neutrons. Indeed, the BC crossing has been observed near 0.31 MeV in ^{171}W [29] and ^{170}Ta [35], which is consistent with this interpretation of the second crossing in Band 2.

Support for the $\pi h_{11/2}\nu AE(F)$ sequence crossing the [404]7/2 band may be observed in Fig. 8(a), where the experimental $B(M1)/B(E2)$ ratios are consistent with the predicted values for the $\pi h_{11/2}\nu AEBC$ configuration (long-dashed line) at spins above 45/2. In contrast, the dot-dashed line representing the $\pi g_{7/2}\nu AB$ configuration is consistently below the experimental values. Additionally, the lack of a crossing near 0.45 MeV (where the E_pF_p alignment is found in Band 1) suggests that Band 2 must have an $h_{11/2}$ proton involved in its configuration such that this crossing is blocked. With this interpretation of Band 2, it is possible that Bands 2a and 2b are the continuation of the [404]7/2 band after the AB alignment. As seen in Fig. 7(b), Bands 2a and 2b initially have the expected alignment of a $\pi g_{7/2}\nu AB$ configuration. The

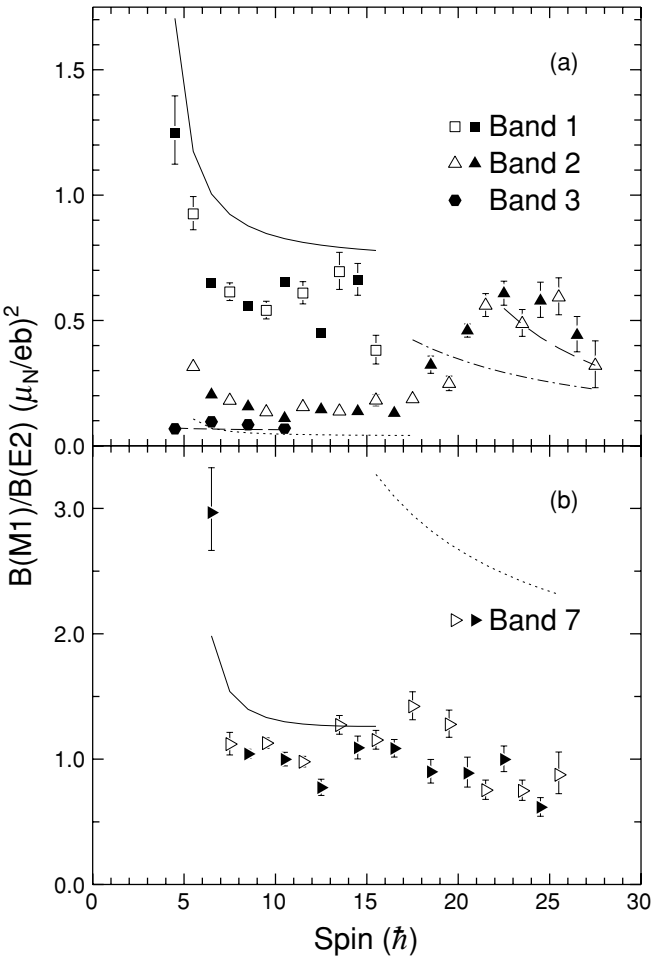

FIG. 8. $B(M1)/B(E2)$ ratios for Bands 1, 2, 3, and 7 in ^{171}Ta. Filled (empty) symbols represent the experimental values for the $\alpha = +1/2$ $(-1/2)$ sequence. (a) The positive-parity bands and the lines represent calculated values for the following configurations: [402]5/2 solid; dotted [404]7/2; $\pi g_{7/2}\nu AB$ dot-dashed; $\pi h_{11/2}\nu AEBC$ long dashed; [411]1/2 dashed. (b) Band 7 with the calculated for the [514]9/2 (solid line) and $\pi h_{11/2}\nu AB$ (dotted line) configurations.

beginning of a crossing is then found in these bands below 0.5 MeV, that is near the frequency of the E_pF_p alignment found in Band 1.

3. The band based on the [411]1/2 orbital

As stated above, Band 3 is a new sequence which exhibits significant signature splitting that can be observed in Fig. 5(a). This suggests that a low-K orbital is likely responsible for this structure. The [411]1/2 orbital is known to be near the tantalum Fermi surface, as it has been seen in ^{169}Ta [36] and ^{173}Ta [37]. The $B(M1)/B(E2)$ ratios, shown in Fig. 8(a), agree with the theoretical predictions (shown as a dashed line), thus Band 3 is assigned the [411]1/2 configuration. Figure 7(a) displays its alignment, and the pattern is similar to that observed in Band 2 in the AB crossing region. Once again, mixing with a more-deformed sequence is assumed to cause this behavior.

TABLE III. The deduced $B(E1)$ transition strengths and electric dipole moments of linking transitions between the [411]1/2 and [541]1/2 bands. A quadrupole moment of 6.0 b was assumed in calculating the $B(E1)$ strengths.

Spin	$E_\gamma(E1)$ (keV)	$E_\gamma(E2)$ (keV)	λ[a]	$B(E1)/B(E2)$ $\times 10^{-8}$ fm^2	$B(E1)$ $\times 10^{-4}$ e^2 fm^2
$\frac{7}{2}$	260.8	173.9	5.68(28)	0.122(6)	0.11(1)
$\frac{11}{2}$	447.1	281.1	7.93(39)	0.191(9)	0.21(2)
$\frac{15}{2}$	607.2	357.6	4.54(21)	0.441(20)	0.51(6)
$\frac{19}{2}$	719.0	409.9	4.40(25)	0.543(31)	0.65(8)
$\frac{23}{2}$	783.0	452.9	4.71(37)	0.647(51)	0.79(10)
$\frac{27}{2}$	816.2	498.1	5.07(23)	0.854(39)	1.06(12)
$\frac{31}{2}$	835.5	544.2	3.40(18)	1.84(10)	2.31(26)

[a]The branching ratio as defined by $\lambda = I_\gamma(E2)/I_\gamma(E1)$.

One may note the strong $E1$ transitions between Bands 3 and 5 seen in Fig. 1. Table III lists the determined $B(E1)/B(E2)$ ratios that were calculated by using the relation

$$\frac{B(E1: I \to I-1)}{B(E2: I \to I-2)} = 0.767 \frac{1}{\lambda} \frac{E_\gamma^5(I \to I-2)}{E_\gamma^3(I \to I-1)}, \quad (1)$$

where λ is the branching ratio. The $B(E1)$ rates were deduced by assuming the rotational form of the $B(E2)$ strength

$$B(E2: I_i \to I_f) = \frac{5}{16\pi} e^2 Q_0^2 \langle I_i K 20 | I_f K \rangle^2, \quad (2)$$

with $Q_0 = 6.0$ b, and the calculated $B(E1)$ strengths are displayed in Table III. The $B(E1)$ values range between 10^{-5} and 10^{-4} e^2 fm^2, which are approximately 100 times stronger than the single-particle strengths calculated for ^{169}Lu [38]. Hagemann, Hamamoto, and Satula [39] investigated the large $B(E1)$ rates in ^{169}Lu and found that octupole correlations

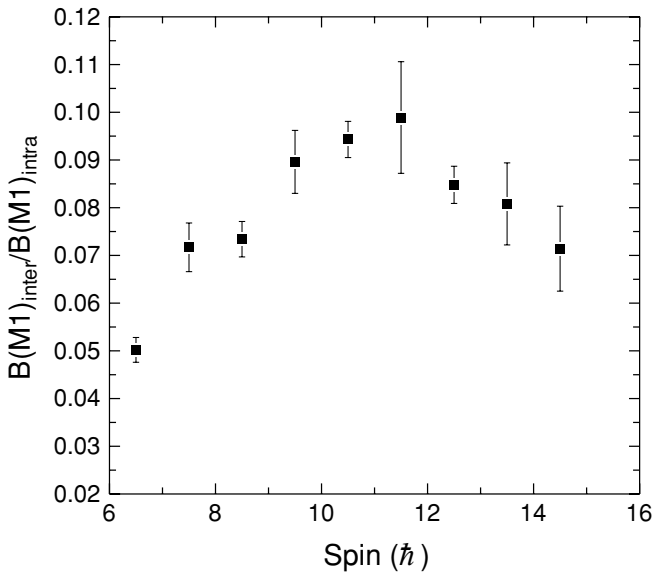

FIG. 9. $B(M1)_{inter}/B(M1)_{intra}$ ratios for linking transitions between Band 1 and 2 deduced from branching ratios.

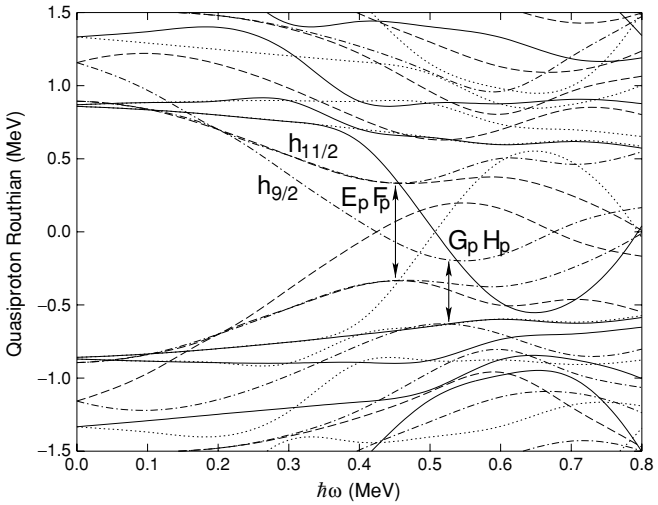

FIG. 10. Cranked shell-model calculations for quasiprotons of ^{171}Ta. Deformation parameters of $\beta_2 = 0.24$, $\beta_4 = 0$, and $\gamma = 1^\circ$ were used. The two lowest frequency crossings are denoted in the figure.

must be invoked to reproduce the large strengths in the latter nucleus. Such correlations are expected when orbitals with $\Delta j = \Delta l = 3$ are near the Fermi surface. This relation is satisfied with Bands 3 and 5 as they are based on the $d_{3/2}$ and $h_{9/2}$ (see below) orbitals, respectively.

Similar to the [404]7/2 band, a relatively low-frequency second crossing is observed at 0.34 MeV. Assuming that this is the same *BC* crossing seen in Band 2, it appears that the [411]1/2 band is also crossed by a three-quasiparticle structure before the *AB* alignment is complete. In Fig. 5(a) one may note that the signature splitting in Band 3 is nearly nonexistent above $I = 39/2$, which is indicative of a structural change as well. This three-quasiparticle band would likely need to have a low K value to mix strongly with the [411]1/2 orbital. Thus, a possible configuration for this band is $\pi h_{9/2} \nu AE(F)$ because it will have a low K value and the *BC* alignment would occur for this configuration. This assignment also explains the reduced signature splitting in Band 3 as the E and F neutrons likely have small splitting, as stated above.

4. The band based on the [660]1/2 orbital

Band 4 has been previously determined to be based on the intruder [660]1/2 orbital [15] because of the large value of its dynamic moment of inertia. A gradual gain in alignment is observed for this band in Fig. 7(c); however, the Harris parameters used are not likely to be appropriate for Band 4, because this sequence may well have enhanced deformation (see below). The dynamic moment of inertia ($J^{(2)}$) for this band, as well as that of the $\pi i_{13/2}$ structures in several nearby nuclei, is presented in Fig. 11. Inspection of the $J^{(2)}$ moment for this sequence in ^{171}Ta reveals that it is nearly constant over a large frequency range. Therefore, there is little indication that any crossing has occurred. In contrast, the Au and Ir $i_{13/2}$ bands displayed in Fig. 11 indicate that two interactions may be present within the frequency range of 0.1–0.5 MeV. A rise in the $J^{(2)}$ values at low frequency has been the subject of several interpretations such as the crossing with a more-deformed band [40] and the alignment of $h_{9/2}$ protons [41]. This is normally followed by the *AB* neutron alignment near 0.4 MeV that accounts for the sharp peaks in $J^{(2)}$ observed in Fig. 11 for the Au and Ir nuclei.

Band 4 more closely resembles the $i_{13/2}$ bands in the Lu nuclei, as seen in Fig. 11. Small peaks in $J^{(2)}$ just above 0.4 MeV can be observed in ^{163,165}Lu and these have been interpreted as the *AB* crossing [3,4]. The rise in the $J^{(2)}$ moment at lower frequencies for ^{161}Lu has also been assigned to the *AB* crossing, followed by an alignment of $j_{15/2}$ neutrons near 0.5 MeV [6]. If these rises are, in fact, due to the

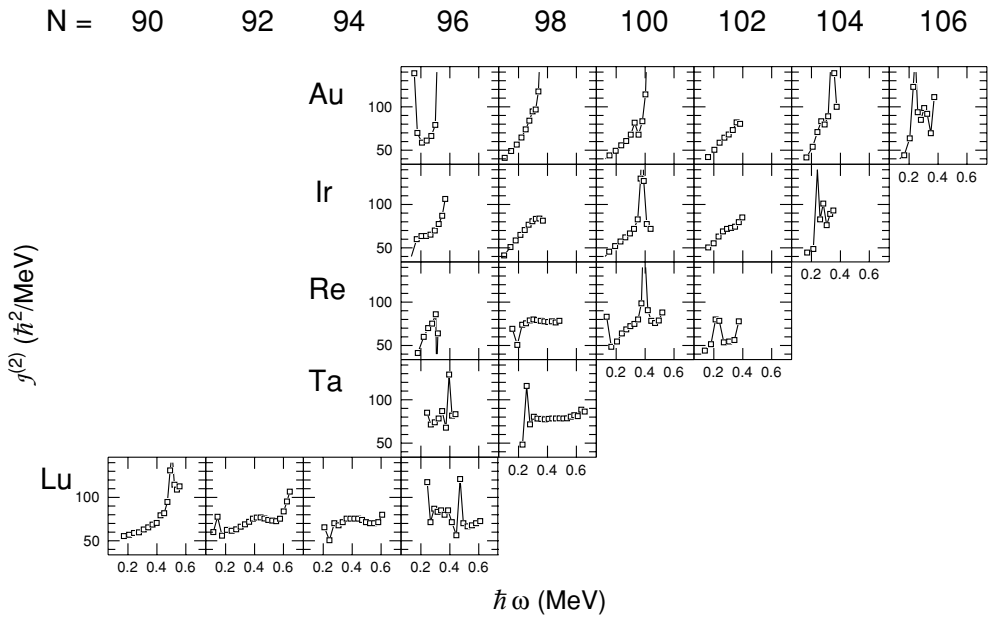

FIG. 11. Dynamic moments of inertia of the $\pi i_{13/2}$ band in the $A \approx 175$ region.

AB alignment, the interaction strength of the associated crossings is clearly larger in the Lu nuclei as compared with the Au and Ir cases because the peaks in Fig. 11 are not nearly as large. This is likely because of the large deformation observed in the $i_{13/2}$ bands of the Lu nuclei [42]. Conversely, there is no clear indication of the *AB* alignment in ^{167}Lu, a situation similar to that found in the $N = 98$ nuclei ^{171}Ta and ^{173}Re.

Perhaps the *AB* interaction strength increases substantially for the Lu, Ta, and Re nuclei when the bands are strongly deformed and, as a result, little or no disturbance is observed in the dynamic moment of inertia. It is not clear why the interaction strength would be so large, although some authors have postulated that it may be ascribed to proton-neutron interactions [43]. Indeed, this type of interaction is expected to strengthen when the proton and the aligning neutrons occupy the *same* orbital as is the case with the $i_{13/2}$ neutrons aligning in the $\pi i_{13/2}$ band. If this is the cause, there is an apparent amplification of the effect in these nuclei, which would deserve further theoretical investigation. An alternative interpretation would be to suggest that the *AB* alignment is greatly delayed in ^{167}Lu, ^{171}Ta, and ^{173}Re. However, an enhanced deformation alone would not explain the delay of this *AB* alignment to frequencies in excess of 0.6 MeV. It is interesting to note that the *AB* crossing occurs near 0.4 MeV in ^{175}Re (see Fig. 11); therefore, the onset of this delay would have to develop suddenly over a small region in neutron number in the Re nuclei. Once again, further theoretical consideration is needed to explain this unusual behavior.

Since Band 4 appears to be similar to the TSD structures in Lu nuclei, an attempt was made to estimate the deformation enhancement. The mixing of the 33/2 states between the [660]1/2 and [404]7/2 bands leads to an estimate of the ratio of the quadrupole moments of the bands assuming pure two-state mixing. As stated in Ref. [44], the mixing amplitude α between the normal deformed (ND) and strongly deformed (SD) states can be determined using the $B(E2)_{\text{inter}}/B(E2)_{\text{intra}}$ ratio of the 37/2 state in Band 4 as follows:

$$\frac{B(E2:565.8)}{B(E2:530.5)} = \frac{\alpha^2}{1-\alpha^2} = \frac{I_\gamma(565.8)}{I_\gamma(530.5)}\left(\frac{530.5}{565.8}\right)^5. \quad (3)$$

Using the intensities given in Table I, one obtains a value of $\alpha^2 = 0.183$ (16). A consistent value of $\alpha^2 = 0.200$ (26) is derived using the same procedure with the 37/2 state in Band 2 as this level has a linking transition to Band 4. The $B(E2)_{\text{inter}}/B(E2)_{\text{intra}}$ ratio out of the mixed 33/2 state is dependent on α^2 as well as on the quadrupole moments of the bands and their Clebsch-Gordon coefficients by the relation:

$$\frac{B(E2:608.8)}{B(E2:496.0)} = \frac{\alpha^2}{1-\alpha^2}\frac{Q_{\text{ND}}^2\langle I_i K_{\text{ND}} 20|I_f K_{\text{ND}}\rangle^2}{Q_{\text{SD}}^2\langle I_i K_{\text{SD}} 20|I_f K_{\text{SD}}\rangle^2} = \frac{I_\gamma(608.8)}{I_\gamma(496.0)}\left(\frac{496.0}{608.8}\right)^5, \quad (4)$$

where $K_{\text{ND}} = 7/2$ and $K_{\text{SD}} = 1/2$. Note that the dependence on the K values occurs only through the Clebsch-Gordon coefficients. A quadrupole moment ratio is then derived to be $Q_{\text{SD}}/Q_{\text{ND}} = 1.67$ (24), which suggests that the $i_{13/2}$ band may have $Q_{\text{SD}} \approx 10$ b assuming $Q_{\text{ND}} = 6.0$ b. This estimate is somewhat larger than the quadrupole moment determined for the $\pi i_{13/2}$ band in ^{173}Re [45]. An average moment of 8.1(5) b was reported, which the authors state as "considerably larger than the $h_{9/2}$ band." Because ^{173}Re is an isotone of ^{171}Ta, a similar moment may be expected for this $i_{13/2}$ band. A residual Doppler shift attenuation method (DSAM) analysis [46] was performed to possibly substantiate this result. However, it was not possible to confirm the proposed enhancement in this manner. A DSAM measurement with a backed target is required to conclusively determine the relative deformations of the various orbitals in ^{171}Ta.

B. Negative-parity bands

1. The bands based on the $h_{9/2}$ orbitals

As seen in Fig. 5(b), large signature splitting is observed for Band 5, which indicates that it is based on a low-K orbital. A large initial alignment of $\sim 3\hbar$ is found in Fig. 7(c) and the *AB* crossing occurs at a frequency of 0.29 and 0.27 MeV for the favored and unfavored signatures, respectively. The delay in the *AB* alignment is known to be a characteristic of [541]1/2 bands and is thought to be at least partially due to increased deformation [30]. Indeed, Joshi *et al.* [47] measured the quadrupole moment of this band to be above 6 b, which is larger than that found for the [514]9/2 band [22]. It is interesting to note that the alignment gain of $5.7\hbar$ for the favored $\alpha = +1/2$ signature is relatively small with respect to that observed in the other bands. Even the unfavored signature of Band 5 has a reduced alignment gain of $7.7\hbar$. Jensen *et al.* [30,45] have noted that the [541]1/2 bands in $N = 98$, odd-Z nuclei systematically exhibit smaller alignment gains, a smaller delay in the *AB* crossing frequency, and a larger interaction strength, but it is not clear why the $N = 98$ nuclei behave so differently from their odd-Z neighbors. A high-frequency crossing is observed in the $\alpha = +1/2$ signature near 0.54 MeV. This is likely the E_pF_p crossing with a very large delay, which is also seen in the $h_{9/2}$ band in ^{169}Ta [48], as well as in the ground-state bands of ^{168,170}Hf [28,49]. The higher deformation of the $h_{9/2}$ bands may play some role as CSM calculations predict a delay of $\sim$0.03 MeV. However, this only accounts for a small part of the 0.12 MeV delay observed, and it does not explain the delay in the even-even Hf nuclei, where enhanced deformation is not expected.

Band 6 is a short sequence with an alignment profile that is very similar to that of the [541]1/2 structure [see Fig. 7(c)]. Perhaps, this is a portion of the next lowest $\pi f_{7/2}/h_{9/2}$ sequence where the completion of the *AB* crossing is observed, as seen in the alignment plot of Fig. 7(c). Woods-Saxon calculations [24] suggest that this orbital lies $\sim$1 MeV above the [541]1/2 orbital, which is consistent with Band 6 lying approximately 800 keV above the favored signature of Band 5, as seen in Fig. 5(b). Another possibility is that Band 6 is a vibrational sequence based on the $h_{9/2}$ proton. Indeed, a similar band in ^{173}Ta [37] has been tentatively assigned as a γ-vibrational sequence based on the [541]1/2 structure. However, the available information is insufficient to propose a confident assignment for this sequence in ^{171}Ta.

2. The band based on the [514]9/2 orbital

Finally, a [514]9/2 assignment has been previously made [15] for Band 7, and the $B(M1)/B(E2)$ ratios shown in Fig. 8(b) are in agreement with theory [shown as a solid line in Fig. 8(b)] for this assignment below $I = 31/2$. The theoretical calculations above the AB crossing, displayed as a dashed line in the figure, significantly overestimate the experimental ratios. This is not understood presently. In addition, note that there is no crossing in the alignment plot [see Fig. 7(d)] near 0.42 MeV for Band 7. This is supportive of the [514]9/2 assignment as the E_pF_p crossing is expected to be blocked when a sequence is based on an $h_{11/2}$ proton. At the highest frequencies observed, one may see the beginning of a crossing, which may be the alignment of the $h_{9/2}$ protons (G_pH_p) as this crossing is predicted to occur near 0.52 MeV in the CSM calculations shown in Fig. 10.

C. Search for a wobbling sequence

As stated above, the primary reason for the study of ^{171}Ta was to search for a wobbling sequence with properties similar to those observed in ^{161,163,165,167}Lu [1–6]. Calculations in Ref. [10] suggested that there may be a TSD gap for $N = 100$, which would then be responsible for the TSD minimum observed in ^{174}Hf [10]. However, questions arose over this possible gap because of the lack of definitive proof of wobbling for the eight SD bands in ^{174}Hf [11]. Therefore, the proximity of ^{171}Ta to $N = 100$, and the fact that the $i_{13/2}$ band was already established, made this nucleus a natural choice to test whether this gap exists. If it does exist at relatively low spins (below $25\hbar$), wobbling sequences should be observed feeding into the $\pi i_{13/2}$ band. In the Lu nuclei, the $n_w = 1$ wobbling sequence is found to have moments of inertia and alignments nearly identical to the $\pi i_{13/2}$ band ($n_w = 0$). The similarity in characteristics is because of the fact that the wobbling sequence has the same intrinsic structure as the $\pi i_{13/2}$ ($n_w = 0$) band. Therefore, an exhaustive search was carried out for a sequence with similar energy spacings as the $\pi i_{13/2}$ band in ^{171}Ta. As seen in Fig. 1, the $i_{13/2}$ sequence has a nearly constant energy spacing of $\sim$51 keV. A search was performed assuming either regular or irregular spacings ranging from 40 to 60 keV. However, no candidate sequence was found.

It is possible that a wobbling band exists, but that it is populated very weakly. If a wobbling band is present in ^{171}Ta, one may infer from Fig. 5(a) that it would compete with at least three other positive-parity sequences that lie within 500 keV of the $i_{13/2}$ band at high spin. However, this situation is no different from that of the wobbling bands in ^{163}Lu, where there is also competition with other normal deformed bands (see Fig. 14 in Ref. [2]), and yet the $n_w = 1$ sequence is observed with one-fourth the intensity of the $i_{13/2}$ band. An intensity upper limit of a possible wobbling sequence in ^{171}Ta, with respect to the strongest transition in the nucleus, was determined to be 0.8%, whereas the $i_{13/2}$ band has an intensity of $\sim$45% (see Table I). In contrast, the $i_{13/2}$ band and its associated wobbling sequence in ^{163}Lu have population intensities of $\sim$10% and $\sim$2.5%, respectively [1]. Because this same $i_{13/2}$ band in ^{171}Ta was populated so strongly, it seems likely that a wobbling band would be observed if it was present.

The lack of a wobbling band in ^{171}Ta suggests that a shell gap does not occur near $N = 100$ at low spin and that the $N = 94$ gap (thought to be responsible for the Lu wobbling bands) does not significantly influence heavier nuclei in the region. Another implication may well be that wobbling will be observed in a very restricted number of nuclei. To date, no such structures have been identified outside the Lu isotopes; this raises questions about the conditions necessary to produce stable triaxial nuclei. Will the only examples be found in the Lu nuclei, in which case the proton number plays the dominant role and the neutron shell gap only has a lesser influence? Or are there other $N = 94$ isotones exhibiting TSD bands? Clearly the Tm and Ta isotopes with $N \approx 94$ should be investigated to see whether wobbling is unique to the $Z = 71$ nuclei.

Recent calculations by Bengtsson and Ryde [50] indicate that at higher frequencies ($\hbar\omega > 0.3$ MeV), a TSD shell gap opens at $N = 97$ and becomes sizable at large deformation ($\epsilon_2 = 0.42$). This large deformation would not be brought about by a simple $i_{13/2}$ configuration, but would likely involve another deformation-driving orbital, such as the $\nu j_{15/2}$ state. Indeed, ultimate cranker calculations indicate that a TSD minimum becomes very low in energy for ^{171}Ta at high spins ($I > 50$). Deformation parameters of $\epsilon_2 = 0.424$ and $\gamma = 16^\circ$ are predicted for this minimum, which is based on the excitation of both the $i_{13/2}$ proton and the $j_{15/2}$ neutron pair. A search for such a structure was also conducted using energy spacings similar to those found in the nearby Hf SD bands, but, once again, no signal for such a sequence was observed.

Another ramification of the lack of an $N = 100$ TSD shell gap is that it provides further confirmation that the Hf SD bands are based on a much different structural minimum than the TSD bands in Lu. Larger quadrupole moments have been measured for the SD bands in ^{174}Hf [11], when compared with the Lu TSD bands [42]. In addition, the recent assignment of the ^{175}Hf SD band involves a seven-quasiparticle configuration that includes the $i_{13/2}$ and $h_{9/2}$ protons along with two $j_{15/2}$ neutrons [13]. These observations combined with the lack of evidence of wobbling in ^{174}Hf and the calculations in Ref. [50] that show no TSD gap near $N = 102$ make it difficult to associate a triaxial shape to the $N \approx 100$ Hf SD nuclei. If these SD bands are not triaxial in nature, then the eight bands seen in ^{174}Hf would have to be based on eight different quasiparticle configurations, all occurring in a potential sufficiently stable in shape to sustain such a large number of excitations. This in turn leads to another puzzling question: If this interpretation holds, how does one account for the fact that only a single SD band was observed in both ^{175}Hf and ^{173}Hf? Naively, one would expect a similar number of SD bands in the odd-A neighbors if multiple combinations of quasiparticle configurations produce SD bands in the even-even neighbors. Clearly, the strongly deformed bands in the heavy rare-earth region are at present not well understood and are in need of further experimental and theoretical investigation.

V. SUMMARY

A search for a wobbling sequence was performed for ^{171}Ta to establish whether stable triaxial deformation could be observed in $N \approx 100$ nuclei. The lack of evidence for such a structure indicates a TSD shell gap most likely does not exist at lower spins, although it is still possible that such a gap occurs at very high spins (>50). In addition, this result further verifies that the SD sequences observed in $N \approx 100$ Hf nuclei have a much different character than the simple $\pi i_{13/2}$ TSD bands found in lighter Lu nuclei. It further raises questions about how broad the region of stable triaxiality actually is. Further experimentation around the $N \approx 94$ nuclei is needed to ascertain the required properties for axial asymmetry.

Although wobbling was not observed in ^{171}Ta, the level scheme was greatly extended in spin. In particular, the $\pi i_{13/2}$ band was observed up to $I = (101/2)$ with a notable regular energy spacing of 51 keV. There is some indication that this band has a large deformation, but a backed-target lifetime experiment must be performed to properly determine the deformation enhancement caused by this intruder orbital. The observation of the blocked *BC* crossing in two bands leads to the interpretation that the [404]7/2 and [411]1/2 sequences are crossed by three-quasiparticle configurations during the *AB* alignment process. A similar crossing has also been found in ^{163,165}Lu [2,32]. Finally, the ground-state spin and parity of ^{171}Ta have been corrected as all the bands have now been linked together. This also establishes for the first time the excitation energies of the the myriad of proton configurations in ^{171}Ta.

ACKNOWLEDGMENTS

Special thanks to D. C. Radford and H. Q. Jin for their software support. The authors wish to thank the ANL operations staff at Gammasphere. Special thanks also to J. P. Greene for target preparation and use. In addition, thanks to Paul T. Mikulski for his help with software issues. This work is funded by the National Science Foundation under grants PHY-0300673 (USNA) and PHY-0139950 (FSU), as well as by the U.S. Department of Energy, office of Nuclear Physics under contracts DE-FG02-96ER40983 (UT) and W-31-109-ENG-38 (ANL).

[1] S. W. Ødegård *et al.*, Phys. Rev. Lett. **86**, 5866 (2001).
[2] D. R. Jensen *et al.*, Nucl. Phys. **A703**, 3 (2002).
[3] D. R. Jensen *et al.*, Phys. Rev. Lett. **89**, 142503 (2002).
[4] G. Schönwaßer *et al.*, Phys. Lett. **B552**, 9 (2003).
[5] H. Amro *et al.*, Phys. Lett. **B553**, 197 (2003).
[6] P. Bringel *et al.*, Eur. Phys. J. A **24**, 167 (2005).
[7] A. Bohr and B. R. Mottelson, *Nuclear Structure*, Vol. II (Benjamin, New York), 1975.
[8] G. B. Hagemann and I. Hamamoto, Nucl. Phys. News **13**, 20 (2003).
[9] H. Schnack-Petersen *et al.*, Nucl. Phys. **A594**, 175 (1995).
[10] M. K. Djongolov *et al.*, Phys. Lett. **B560**, 24 (2003).
[11] D. J. Hartley *et al.*, Phys. Lett. **B608**, 31 (2005).
[12] W. C. Ma *et al.*, private communication.
[13] D. T. Scholes *et al.*, Phys. Rev. C **70**, 054314 (2004).
[14] C. X. Yang *et al.*, Phys. Lett. **B133**, 39 (1983).
[15] J. C. Bacelar *et al.*, Nucl. Phys. **A442**, 547 (1985).
[16] I. M. Ladenbauer-Bellis and I. Rezanka, Atomkernenergie **23**, 279 (1974).
[17] F. Meissner, W.-D. Schmidt-Ott, V. Freystein, T. Hild, E. Runte, H. Salewski, and R. Michaelsen, Z. Phys. A **337**, 45 (1990).
[18] R. V. F. Janssens and F. S. Stephens, Nucl. Phys. News **6**, 9 (1996).
[19] M. Cromaz *et al.*, Nucl. Instrum. Methods A **462**, 519 (2001).
[20] D. C. Radford, Nucl. Instrum. Methods A **361**, 297 (1995).
[21] K. Starosta *et al.*, Nucl. Instrum. Methods A **515**, 771 (2003).
[22] R. Dogra, J. Goswami, A. K. Bhati, S. C. Bedi, and R. K. Bhowmik, Hyperfine Interact. **96**, 223 (1995).
[23] C. M. Baglin, Nucl. Data Sheets **96**, 399 (2002).
[24] W. Nazarewicz, M. A. Riley, and J. D. Garrett, Nucl. Phys. **A512**, 61 (1990).
[25] F. Dönau, Nucl. Phys. **A471**, 469 (1987).
[26] R. D. Ratna Raju, J. P. Draayer, and K. T. Hecht, Nucl. Phys. **A202**, 433 (1973).
[27] R. Bengtsson, S. Frauendorf, and F.-R. May, At. Data Nucl. Data Tables **35**, 15 (1986).
[28] J. Irwin *et al.*, Daresbury Lab., 1988–1989 Ann. Rept. Appendix, 79 (1989).
[29] J. Espino *et al.*, Nucl. Phys. **A567**, 377 (1994).
[30] H. J. Jensen *et al.*, Nucl. Phys. **A695**, 3 (2001).
[31] R. A. Bark, J. Phys. G **17**, 1209 (1991).
[32] G. Schönwaßer *et al.*, Nucl. Phys. **A735**, 393 (2004).
[33] W. B. Gao, I. Y. Lee, C. Baktash, R. Wyss, J. H. Hamilton, C. M. Steele, C. H. Yu, N. R. Johnson, and F. K. McGowan, Phys. Rev. C **44**, 1380 (1991).
[34] D. M. Cullen *et al.*, Nucl. Phys. **A673**, 3 (2000).
[35] A. Aguilar *et al.*, in preparation.
[36] S. G. Li *et al.*, Nucl. Phys. **A555**, 435 (1993).
[37] H. Carlsson *et al.*, Nucl. Phys. **A592**, 89 (1995).
[38] S. Ogaza *et al.*, Nucl. Phys. **A559**, 100 (1993).
[39] G. B. Hagemann, I. Hamamoto, and W. Satula, Phys. Rev. C **47**, 2008 (1993).
[40] G. D. Dracoulis, R. A. Bark, A. E. Stuchbery, A. P. Byrne, A. M. Baxter, and F. Riess, Nucl. Phys. **A486**, 414 (1988).
[41] V. P. Janzen *et al.*, Phys. Rev. Lett. **61**, 2073 (1988).
[42] A. Görgen *et al.*, Phys. Rev. C **69**, 031301(R) (2004).
[43] H. J. Jensen *et al.*, Z. Phys. A **359**, 127 (1997).
[44] J. Domscheit *et al.*, Nucl. Phys. **A660**, 381 (1999).
[45] N. R. Johnson *et al.*, Phys. Rev. C **55**, 652 (1997).
[46] B. Cederwall *et al.*, Nucl. Instrum. Methods A **354**, 591 (1995).
[47] P. Joshi, G. Mukherjee, A. Kumar, R. P. Singh, S. Muralithar, S. C. Pancholi, C. R. Praharaj, U. Garg, R. K. Bhowmik, and I. M. Govil, Phys. Rev. C **60**, 034311 (1999).
[48] D. J. Hartley *et al.*, in preparation.
[49] E. M. Beck *et al.*, Z. Phys. A **327**, 397 (1987).
[50] R. Bengtsson and H. Ryde, Eur. Phys. J. A **22**, 355 (2004).